NANO · MICRO small
www.small-journal.com

Mechanical Processing of Naturally Bent Organic Crystalline Microoptical Waveguides and Junctions

Vuppu Vinay Pradeep, Carlos Tardío, Iván Torres-Moya, Ana M. Rodríguez, Avulu Vinod Kumar, Mari Annadhasan, Antonio de la Hoz, Pilar Prieto, and Rajadurai Chandrasekar**

Precise mechanical processing of optical microcrystals involves complex microscale operations viz. moving, bending, lifting, and cutting of crystals. Some of these mechanical operations can be implemented by applying mechanical force at specific points of the crystal to fabricate advanced crystalline optical junctions. Mechanically compliant flexible optical crystals are ideal candidates for the designing of such microoptical junctions. A vapor-phase growth of naturally bent optical waveguiding crystals of 1,4-bis(2-cyanophenylethynyl)benzene (1) on a surface forming different optical junctions is presented. In the solid-state, molecule 1 interacts with its neighbors via C—H···N hydrogen bonding and π–π stacking. The microcrystals deposited at a glass surface exhibit moderate flexibility due to substantial surface adherence energy. The obtained network crystals also display mechanical compliance when cut precisely with sharp atomic force microscope cantilever tip, making them ideal candidates for building innovative T- and Δ-shaped optical junctions with multiple outputs. The presented micromechanical processing technique can also be effectively used as a tool to fabricate single-crystal integrated photonic devices and circuits on suitable substrates.

Traditionally, crystals are viewed as brittle and hard materials. Exceptionally/surprisingly, some crystals display extraordinary flexibility and softness due to their atypical molecular arrangements.[1] The crystal flexibility (elasticity or plasticity) mainly arises as a result of the interlocked host structure, weak, and dispersive interactions and mobile solvent channels.[1–4] Naturally, some crystals evolve into various twisted or bent geometries during their growth.[5a] The operating stress in bulk or at the surface of the crystal is the driving forces for the unusual shape evolution of these peculiar crystals. A similar mechanism is also driving the formation of bent crystals during solvent-assisted self-assembly on surfaces.[6] Earlier, Hosseini and Naumov et al. reported a solution-based epitaxial growth technique to weld homo- and hetero-type optical waveguiding molecular crystals.[5b] The vapor-phase growth of crystals on a surface is a clean technique. At high concentration (molecular deposition rate), vapor-phase growth might facilitate natural welding and diverse junction formation between the crystals depending upon lattice matching and mismatching possiblites, respectively. As this idea has not been tested in the literature, we envisaged vapor-phase growth of bent crystals at high concentration with diverse bent angles to produce intricate crystal junctions.

Flexible crystals are also known for their extraordinary photonic attributes viz. optical waveguides,[7] cavities,[8] lasers,[9] circuits,[10] field-effect transistors,[11] modulators,[12] polarization rotors,[13] and wavelength division multiplexers.[14d] A combination of flexibility and optical traits makes this class of peculiar-crystals prospective candidates for the fabrication of single-crystal-based optical junctions useful in multidirectional optical communication technologies. However, precise mechanical processing of naturally bent crystals and junctions into desirable configuration is a challenging task, and to our knowledge, no reports accomplished this task. Till now, the dimensions of most of the studied crystals possessing both flexibility and light guiding attributes are in the range of millimeters.[3] The mechanical properties of such macrocrystals were demonstrated by using tweezers.[2] The technique of precise manipulation of photonic microcrystals using atomic force microscopy (AFM)—mechanophotonics,[14] is a recent technical development in the area of flexible crystal-based photonics. This technique can be extended to process single-crystal-based optical junctions mechanically down to microscale.

V. Vinay Pradeep, A. Vinod Kumar, Dr. M. Annadhasan, Prof. R. Chandrasekar
School of Chemistry
University of Hyderabad
Prof. C. R. Rao Road, Gachibowli, Hyderabad 50046, India
E-mail: r.chandrasekar@uohyd.ac.in

V. Vinay Pradeep, A. Vinod Kumar, Dr. M. Annadhasan, Prof. R. Chandrasekar
Centre for Nanotechnology
University of Hyderabad
Prof. C. R. Rao Road, Gachibowli
Hyderabad 50046, India

C. Tardío, Dr. I. Torres-Moya, Dr. A. M. Rodríguez, Prof. A. de la Hoz, Prof. P. Prieto
Department of Biochemistry
Organic and Inorganic Chemistry
Faculty of Chemical and Technologies Sciences
University of Castilla- La Mancha
Ciudad Real 13071, Spain
E-mail: mariapilar.prieto@uclm.es

The ORCID identification number(s) for the author(s) of this article can be found under https://doi.org/10.1002/smll.202006795.

DOI: 10.1002/smll.202006795

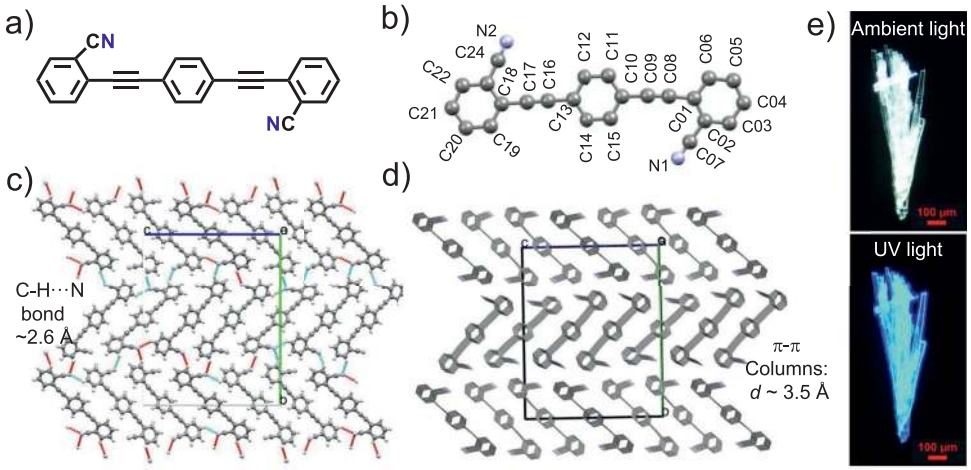

Figure 1. a) Molecular structure of **1**. b) The single-crystal X-ray structure of **1**. The H-atoms are omitted for clarity. c,d) The molecular packing diagram of **1** in the solid-state forming H-bonding and π–π interactions. e) Photograph of crystals of **1** under normal light ad UV light, respectively.

We have previously reported alkynyl derivatives with heterocyclic cores that form supramolecular aggregates and show optical waveguiding properties. The presence of rod-like molecules and weak intermolecular interactions, such as hydrogen bonds, and π-stacking could provide crystal flexibility.[15] Consequently, we describe here a linear alkynyl derivative with a benzene core, namely, 1,4-bis(2-cyanophenylethynyl)benzene (**1**) and for the first time, report precise mechanical processing of naturally bent flexible crystals into photonic circuit configurations using AFM cantilever tip (**Figure 1**a). We demonstrate i) the mechanistic insights into the natural crystal welding process which leads to the formation of exceptionally bent and complex crystal junctions, ii) mechanical compliance of low optical loss crystal waveguides for AFM manipulation from bent to straight geometries, and iii) precise cutting of photonic circuits into T- and Δ-geometries with three and four optical outputs, respectively.

Compound **1** was prepared by using Stille cross-coupling reaction under microwave irradiation in 70% yield (Figures S1 and S2, Supporting Information). Needle-shaped single crystals suitable for X-ray analysis were obtained by slow diffusion of methanol in tetrahydrofuran solution of **1** (Figure 1e). The solid-state packing shows π–π stacking of each molecule with a distance of 3.936 Å. Each molecule intermolecularly interacts via C—H···N (cyano) hydrogen bonding with a distance of 2.602 Å (Figure 1c,d). This weak interaction defines a slip plane orthogonal to the (011) plane (see the dotted red lines in Figure 2d).

The compound **1** was sublimed on to a glass coverslip (Borosilicate, contact angle ≈48°) at ambient pressure at 140 °C, which resulted in both straight and naturally bent microrods.[16] Interestingly, the confocal microscopy images of the sublimed microrods showed the formation of several bent rods interconnected to each other forming circuits (**Figure 2**a). Three representative bent microrods with different bent angles viz., 160°, 140°, and 90° are shown in the field emission scanning microscope (FESEM) images (Figure 2c). Investigation of the mechanism of formation of naturally bent rods with different bent angles revealed fusion of two straight rods forming bent structures. The fusion or welding of straight rods into the bent configuration is facilitated by the facet-matching of two rods at their intersection point, as shown in Figure 2d–j. As expected, the polarizing microscope images revealed difference in contrast for the bent area compared to the rest of the rod due to dissimilarity in the molecular orientation direction with respect to the analyzer (Figure S4, Supporting Information). The bent angle is dependent upon the growth direction of the two straight rods. For example, the formation of a bent rod with 90° angle shows near orthogonal growth of two rods until they bump into each other and fuse. In case of rods with ≈160° and ≈140° bent angles, the angle of intersection between the growth trajectories of the two rods is ≈160° and ≈140°, respectively. Similarly, a bent rod growing near the orthogonal direction of another rod form facet mismatched junctions, wherein the mismatching of the facets halted the growth of one of the microrods (Figure 2a). The degrees of freedom available due to the presence of slip planes and π–π stacking interactions favor the fusion of the two rods which are approaching each other at various angles.

To probe the optical waveguiding propensity of straight microrods, a single rod of length, L ≈17.6 µm (**Figure 3**a), was excited at the corner of one of the termini with a 405 nm laser (Figure 3b). As a result, the microrod generated a bright blue fluorescence (FL) at the point of excitation that transduced through its long axis to the opposite terminal with a brilliant outcoupled emission (Figure 3b). Remarkably, the FL image of the waveguide revealed real-time multiple total internal reflections (TIR) of the emitted optical beam at the air-crystal interface to reach the output terminal (Figure S5, Supporting Information).

The optical loss of the active waveguide was estimated using a representative rod of length ≈16.8 µm. For that, optical excitation at different positions (11.8, 8.4, 5.9, 4.2, 2.5 µm) was performed along the long axis of the rod, and the corresponding FL spectra were recorded at the left end of the microrod (Figure 3c). The obtained FL spectra also comprised of optical modes-like features. As the distance of the propagation of light decreases, the spectra showed a progressive increase of

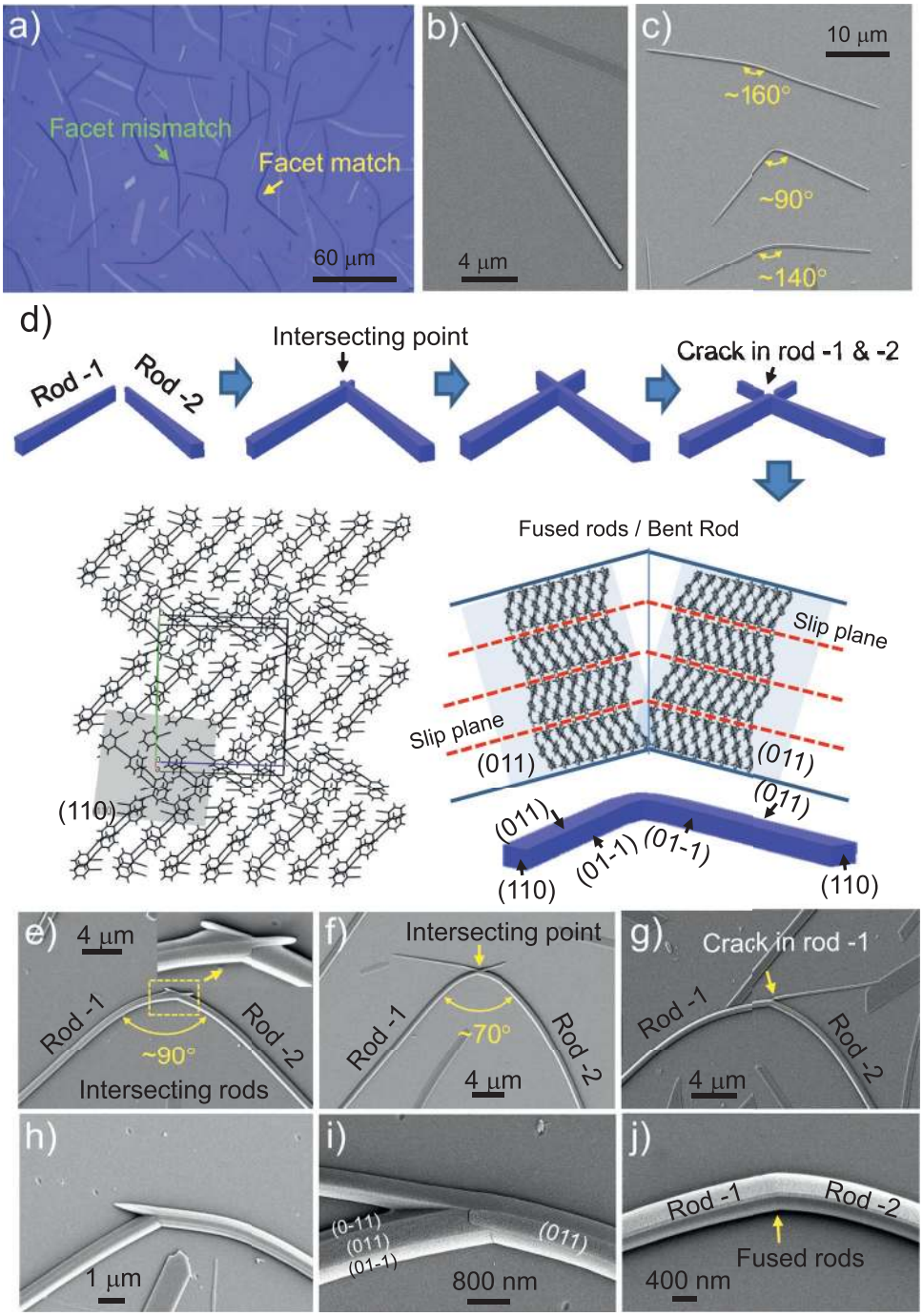

Figure 2. a) Optical microscope image of straight and naturally bent interconnected microrods of **1**. b) FESEM image of a straight microrod. c) FESEM image of three bent rods with different bent angles. d) Cartoon representation depicting the formation mechanism of a naturally bent rod. e,f,h,i) FESEM image of two intersecting microrods at different angles during their growth with the rate of growth. g) Cracking of rods which are not part of bent microrod. j) Formation of a bent microrod via fusion of matching facets.

FL intensity (Figure 3d). The optical loss of the microrod was calculated using an equation $I_{out} = I_{in}\, e^{-\alpha d}$, where I_{out} and I_{in} are the FL intensities at the output and input, respectively, d is the propagation distance, and α is the optical loss coefficient in mm^{-1}. The value calculated after converting α to dB mm^{-1} (by using the relation $\alpha'/(\text{dB mm}^{-1}) \approx 4.34\ \alpha/\text{mm}^{-1}$) is 0.4967 dB μm^{-1}.

To further confirm the presence of optical modes in the FL spectra, several microrods of various lengths were taken and excited with a laser. The resultant FL spectra exhibited mode-like features. The decrease in the length of the rod (14.4, 10.8, 8.9, 6.1, and 5.3 μm) increased the free spectral range (FSR) value (the distance between two successive modes) as per FSR≈1/L relation (**Figure 4**). This result also proves that the

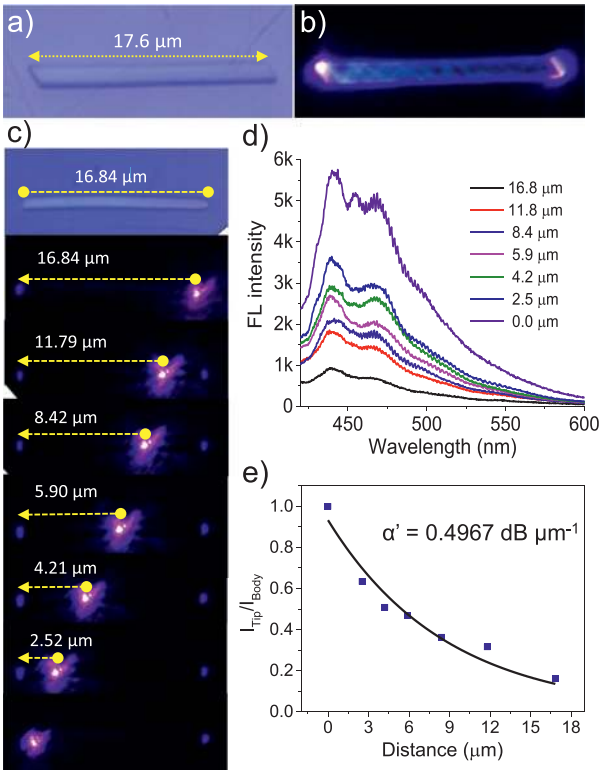

Figure 3. a) Confocal microscope image of a single micro rod. b) FL image of the microrod showing the TIR. c) FL images of a microrod transducing light when they are excited at different positions. The yellow dotted arrows indicate the direction of light propagation. d) The corresponding FL spectra of the microrod when excited at different positions. e) A plot of the intensity ratio at the tip and the body of the crystal (I_{tip}/I_{body}) versus the distance of the light propagation path used to estimate the optical loss coefficient (α).

trapped optical light within the microrod travels back and forth due to the mirror-like reflective surface of the smooth facet at the termini. Subsequently, this effective light reflection enhances optical interferences and generated Fabry–Perot resonances.

To probe the flexibility of microrods, a longer rod was cut in two places (C-1 and C-2) using an AFM cantilever tip to create three single-crystal rods of varying lengths (**Figure 5**a). Cantilever force (F) was applied to one of the terminals of the rod of length (L ≈ 36.6 µm) to bend that terminal to about 5.26 µm from its original position (Figure 5b). Due to possible adhesion with the surface, the bent rod retained its curved shape even after the removal of the force (Figure 5c). To study the optical loss due to crystal bending, the rod was excited at the left terminal, and the FL spectra were collected at the opposite output terminal (Figure 5i). Further, when the rod was excited nearly at the middle and at the right terminal of the rod, the FL spectra were collected at the right output terminal. The obtained spectra confirmed transmission of FL through the bent microrod. As expected, when the path distance decreases, the FL intensity progressively increased (Figure 5k). Again, the bent rod was made nearly straight by applying the cantilever pull and push forces (Figure 5d–g). The FESEM image of the straightened rod revealed no damages due to mechanical bending and straightening operations (Figure 5h,l). The excitation position-dependent FL spectra were recorded on this microrod similar to the bent rod. The FL intensity for both the cases (bent and straight) show similar emission intensity at all the excitation positions, which confirms a negligible optical loss in the rod due to mechanical bending (Figure 5k).

We explored the possibility of creating optical junctions from a naturally bent interconnected network. For that, we have identified a network forming a nearly T-shaped junction (**Figure 6**a).

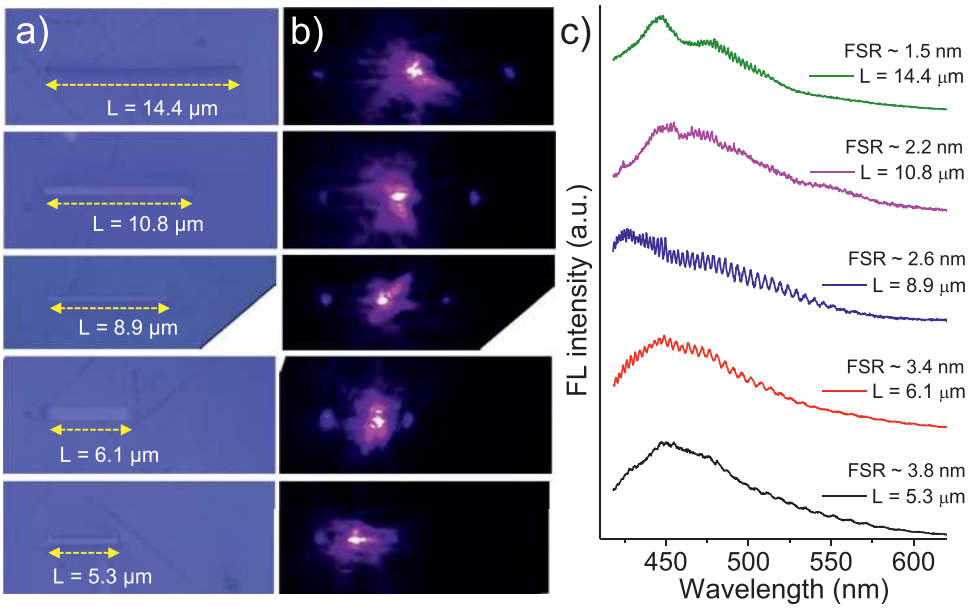

Figure 4. a) Confocal microscope images, b) FL images, and c) FL spectra of different microrods of different lengths. The spectra show an increase in FSR with a decrease in the length of microrod.

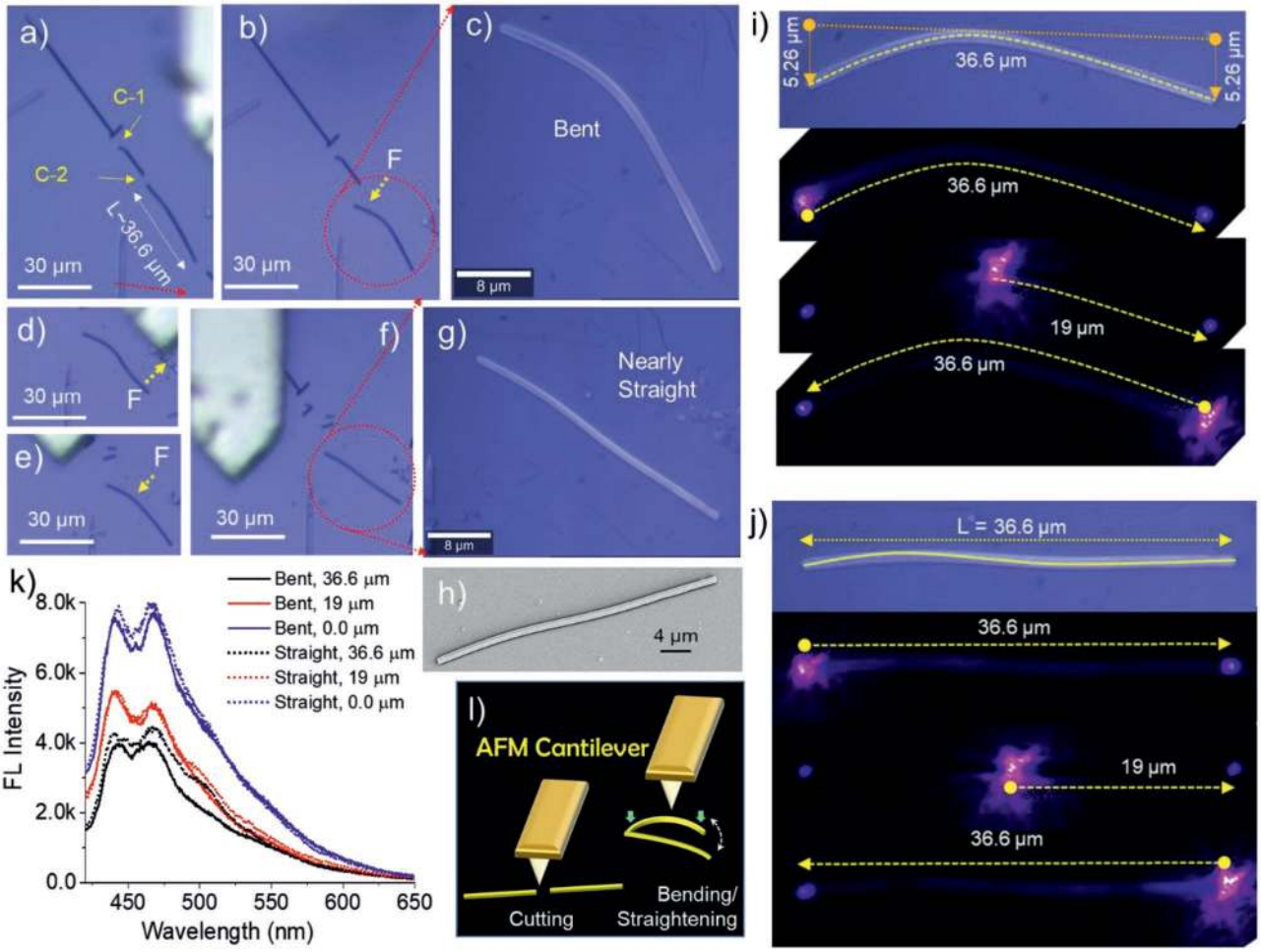

Figure 5. a,b) Confocal microscope images while performing breaking and bending of the microrod with AFM cantilever force. The broken arrows show applied force (F) directions. c) Confocal image of a mechanically bent rod. d–f) Straightening of the bent rod with AFM cantilever force. g) Confocal image and h) FESEM image of mechanically straightened microrod. i,j) FL images of straight and bent rod transducing light when they are excited at different positions. k) FL spectra of straight and bent rod when they are excited at different positions, respectively. l) Graphical representation of cutting and bending/straightening of microrod.

The three long arms of the network were cut (C1-C3) by AFM cantilever in three steps (Figure 6b–d) to produce a nearly T-shaped optical junction (Figure 6e). The resultant junction has three outputs/inputs (labeled 1–3) and a junction (J1). The lengths of the long arm (from 1 to 3) is 15 µm, whereas the shorter arm has a length of 8 µm (Figure 6l). Initially, the circuit was excited at terminal 1. As a result, a bright FL output was observed at terminal 3, and weaker FL at terminal 2 (Figure 6f). The FL spectra are given in Figure 6j. The representation is made as 1-2 and 1-3, which mean excitation at terminal 1 and FL detection at terminal 2 and 3, respectively. Similarly, the circuit was excited at all terminals (2 and 3) and FL spectra were detected at outputs viz., 2-1, 2-3, and 3-1, 3-2, respectively. Finally, excitation at the junction (J1) of the circuit produced FL output at all the terminals (J1-1, J1-2, J1-3). The spectral emission features were similar in all outputs with varying intensities, which indicate that the T-circuit can be used to split the light into two parts which are propagating in an orthogonal direction (Figure 6l). The optical function of the T-shaped junction is summarized in Figure 6k.

Additionally, we found an assembly of three bent rods (I-III) with bent angles of ≈170°, ≈130°, and ≈90°, respectively producing a triangular-shaped junction around their interconnection points (**Figure 7**a). Bent rod I is connected to II and III, while the latter two rods are not directly connected with each other. The triangle does not represent a closed-loop as the rods II and III are not interconnected. To disconnect the triangular part from the interconnected bent rods selectively, the rods were cut (C1-C3) using the AFM cantilever tip in three steps (Figure 7b–d). The finally crafted triangular-shaped microjunction using micromanipulation technique consists of three straight waveguides (I-III) of length 19.4, 18.3, and 17.1 µm (Figure 7e,l). The junction also possesses four output/input terminals (1-4) and two junctions, namely J1 and J2. The junction was excited (with a power of 1 mW) at position J1, and the FL signal was detected at positions 1, 4, and J2 (Figure 7f). Excitation at position J2 exhibited FL outputs at 1, 2, 3, and J1 (Figure 7g). Excitation at terminal 1 showed FL output only at J1 and J2 (Figure 7h). For the input at terminal 2, the FL outputs were detected at J2 and 3 (Figure 7i). Excitation at input

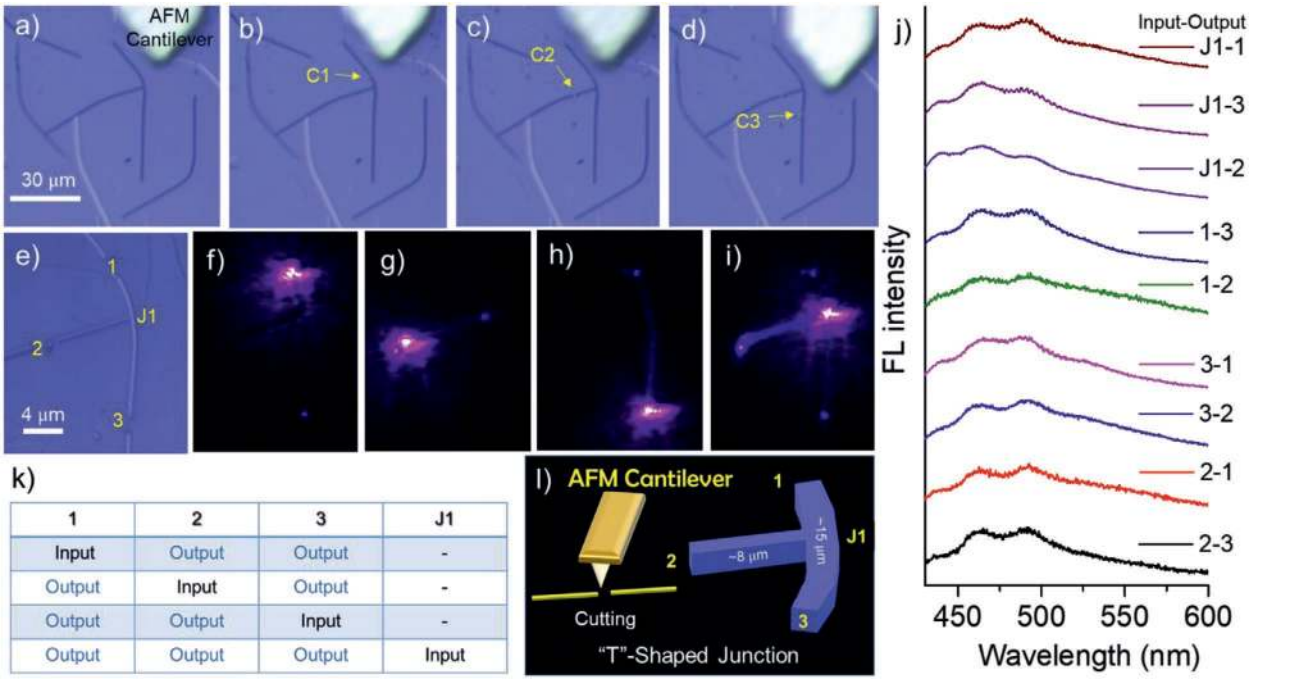

1	2	3	J1
Input	Output	Output	-
Output	Input	Output	-
Output	Output	Input	-
Output	Output	Output	Input

Figure 6. a) Confocal image of three interconnected bent rods forming a network. b–d) Reducing the length of the microrods to create a T-shaped junction. e) A T-shaped junction with three optical inputs/outputs and one junction (J1). f–i) FL images of the junction when excited at different terminals. j) FL spectra collected at different termini when excited at one position. k) Table depicts various input and output positions. l) Graphical representation of T-shaped microrod crafted by precisely cutting with AFM cantilever tip.

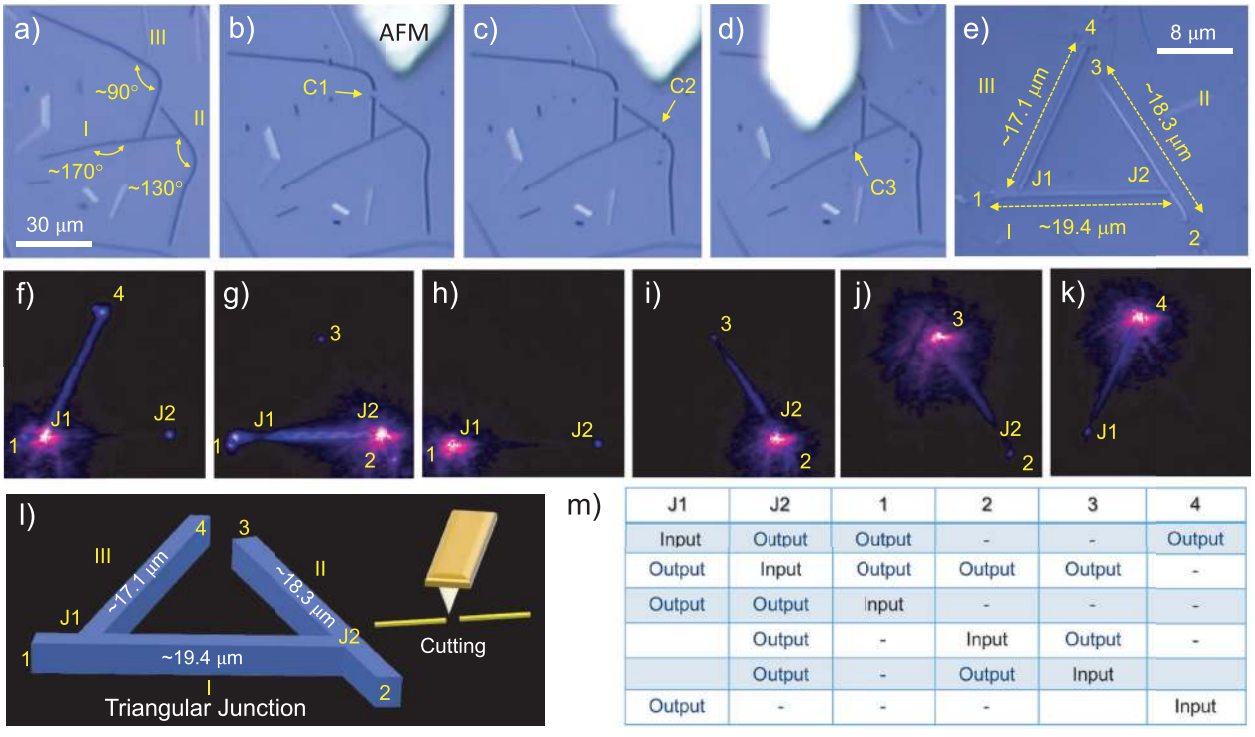

J1	J2	1	2	3	4
Input	Output	Output	-	-	Output
Output	Input	Output	Output	Output	-
Output	Output	Input	-	-	-
	Output	-	Input	Output	-
	Output	-	Output	Input	
Output	-	-	-		Input

Figure 7. a) Confocal microscope image of three intersecting bent rods (I-III) of different bent angles forming a triangle-shaped microjunctions at the intersecting point. b–d) Confocal microscope images exhibiting creation of a microjunction by cutting at three places (C1-C3) using AFM cantilever tip. e) Confocal image of engineered triangular microjunction with four optical inputs/outputs and two junctions (J1 and J2). f–k) FL images of microjunction when excited at different positions. l) Schematic side-view representation of the triangular circuit fabricated using micromanipulation using AFM cantilever tip. m) Table showing the optical outputs for an input.

3 produced FL outputs at J2 and 2 (Figure 7j). Excitation at input 4, only showed output at J1 (Figure 7k). The table given in Figure 7m summarizes the optical function of triangular micro-junction. The corresponding FL spectra are given in Figure S6 (Supporting Information).

In summary, the fabrication of blue-emitting linear and naturally bent interconnected microcrystal waveguides of **1** with different bent angles was demonstrated using a vapor-phase growth technique. For the first time, the mechanistic analysis revealed that the formation of naturally bent waveguides as a result of the intersection of two growing crystals toward each other at different angles and their fusion along the matching facets forming a bent single crystal. Further, the waveguides revealed the TIR of FL light and also FP cavity resonances. Most of the crystal waveguides could be mechanically straightened or bent using AFM micromanipulation technique. The mechanically compliant waveguides also exhibited low optical loss both in bent and straight geometry. Mechanical processing with AFM cantilever tip allowed precise cutting of the interconnected bent waveguides at desired locations. The resultant T- and triangular-shaped optical junctions facilitated the flow of optical signal(s) at different angles in two dimensions depending upon the optical excitation position. The presented proof-of-principle experiments which combine state-of-the-art mechanical processing and photonic studies of flexible microcrystals demonstrate the potential of the presented technique in the area of mechanophotonics.[14]

Experimental Section

Synthesis of 2-((tributylstannyl)ethynyl)benzonitrile (3):

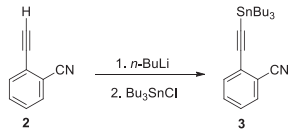

Butyllithium (1.27 mL, 5.895 mmol, 1.6 M in hexane) was added dropwise under an inert atmosphere to a stirred solution of 2-ethynylbenzonitrile (**2**) (0.5 g, 3.93 mmol) in dry THF at –78 °C. The mixture was stirred 10 min, and tributylchlorostannanel (4.72 mL, 1.27 mmol) was added dropwise. The mixture was allowed to reach room temperature and was stirred for 2 h. Then 30 mL of water was added to the crude reaction mixture, and neutralized with 1 M HCl. The mixture was extracted with CH_2Cl_2 (2 × 20 mL), the organic layers were dried with $MgSO_4$ and concentrated in vacuo. A brown liquid was obtained (1.491 g, 91%). ^{1}H-NMR (500 MHz $CDCl_3$-d_3, δ): 7.60 (d, 1H, J = 7.5 Hz), 7.51 (m, 2H), 7.34 (t, 1H, J = 7.6 Hz), 1.61 (t, 6H, J = 7.6 Hz), 1.38 (m, 6H), 1.07 (m, 6H), 0.93 (t, 9H, J = 7.2 Hz).

Synthesis of 1,4-bis(2-cyanophenylethynyl)benzene (1):

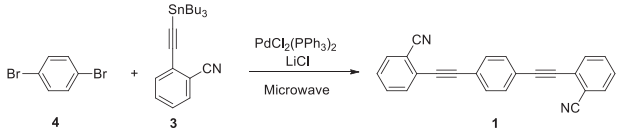

A mixture 1,4-dibromobenzene (**4**) (0.100 g, 0.424 mmol), 2-((tributylstannyl)ethynyl)benzonitrile (**3**) (0.441 g, 1.06 mmol), $PdCl_2(PPh_3)_2$ (0.012 g, 0.016 mmol), LiCl (0.054 g, 1.27 mmol), and CH_3CN (1 mL) was charged under argon to a microwave vessel. The vessel was closed and irradiated at 115 °C for 20 min (CEM Discover, temperature controlled power). The crude reaction was purified by chromatography, eluting with hexane/ethyl acetate 6:1, obtaining a pale yellow solid (0.097 g, 70%). M. p.: 198–199 °C. ^{1}H-NMR (500 MHz $CDCl_3$-d_3, δ): 7.69 (d, 2H, J = 7.6 Hz), 7.62 (m, 6H), 7.59 (td, 2H, J = 8, 1.3 Hz), 7.44 (td, 2H, J = 7.6, 1.3 Hz). ^{13}C-NMR (125 MHz $CDCl_3$-d_3, δ): 132.7, 132.4, 132.1, 132.0, 128.5, 126.8, 122.9, 117.5, 115.4, 95.3, 87.7.

Supporting Information

Supporting Information is available from the Wiley Online Library or from the author.

Acknowledgements

V.V.P. and C.T. have equally contributed to this work. This work was financially supported by DST (New Delhi; Grant No. INT/RUS/RSF/P-05), SERB (No. CRG-2018/001551), UoH-IoE (UoH-IoE/RC1/RC1/20-003) and Junta de Comunidades de Castilla-La Mancha (JCCM-FEDER) Project No. SBPLY/17/180501/000189.

Conflict of Interest

The authors declare no conflict of interest.

Keywords

flexible crystals, mechanophotonics, optical junctions, optical waveguides, vapor-phase growth

Received: November 1, 2020
Revised: December 7, 2020
Published online:

[1] a) S. Saha, M. K. Mishra, C. M. Reddy, G. R. Desiraju, *Acc. Chem. Res.* **2018**, *51*, 2957; b) S. Ghosh, M. K. Mishra, S. B. Kadambi, U. Ramamurty, G. R. Desiraju, *Angew. Chem., Int. Ed.* **2015**, *54*, 2674; c) M. K. Panda, S. Ghosh, N. Yasuda, T. Moriwaki, G. D. Mukherjee, C. M. Reddy, P. Naumov, *Nat. Chem.* **2015**, *7*, 65; d) L. Pejov, M. K. Panda, T. Moriwaki, P. Naumov, *J. Am. Chem. Soc.* **2017**, *139*, 2318; e) P. Commins, D. P. Karothu, P. Naumov, *Angew. Chem., Int. Ed.* **2019**, *58*, 10052.

[2] a) S. Dey, S. Das, S. Bhunia, R. Chowdhury, A. Mondal, B. Bhattacharya, R. Devarapalli, N. Yasuda, T. Moriwaki, K. Mandal, G. D. Mukherjee, C. M. Reddy, *Nat. Commun.* **2019**, *10*, 3711; c) M. Đaković, M. Borovina, M. Pisačić, C. B. Aakeröy, Ž. Soldin, B. M. Kukovec, I. Kodrin, *Angew. Chem., Int. Ed.* **2018**, *57*, 14801; d) A. Worthy, A. Grosjean, M. C. Pfrunder, Y. Xu, C. Yan, G. Edwards, J. K. Clegg, J. C. McMurtrie, *Nat. Chem.* **2018**, *10*, 65.

[3] a) S. Hayashi, T. Koizumi, *Angew. Chem., Int. Ed.* **2016**, *55*, 2701; b) H. Liu, Z. Lu, Z. Zhang, Y. Wang, H. Zhang, *Angew. Chem., Int. Ed.* **2018**, *57*, 8448; c) R. Huang, C. Wang, Y. Wang, H. Zhang, *Adv. Mater.* **2018**, *30*, 1800814; d) L. Catalano, D. P. Karothu, S. Schramm, E. Ahmed, R. Rezgui, T. J. Barber, A. Famulari, P. Naumov, *Angew. Chem., Int. Ed.* **2018**, *57*, 17254; e) J. M. Halabi, E. Ahmed, L. Catalano, D. P. Karothu, R. Rezgui, P. Naumov, *J. Am. Chem. Soc.* **2019**, *141*, 14966.

[4] a) S. Saha, G. R. Desiraju, *J. Am. Chem. Soc.* **2017**, *139*, 1975; b) G. R. Krishna, R. Devarapalli, G. Lal, C. M. Reddy, *J. Am. Chem.*

Soc. **2016**, *138*, 13561; c) J. Harada, T. Shimojo, H. Oyamaguchi, H. Hasegawa, Y. Takahashi, K. Satomi, Y. Suzuki, J. Kawamata, T. Inabe, *Nat. Chem.* **2016**, *8*, 946; d) S. Takamizawa, Y. Takasaki, T. Sasaki, N. Ozaki, *Nat. Commun.* **2018**, *9*, 3984; e) B. Kahr, M. D. Ward, *Nat. Chem.* **2018**, *10*, 4; f) L. O. Alimi, P. Lama, V. J. Smith, L. J. Barbour, *Chem. Commun.* **2018**, *54*, 2994; g) S. Hu, M. K. Mishra, C. C. Sun, *Chem. Mater.* **2019**, *31*, 3818.

[5] a) A. G. Shtukenberg, Y. O. Punin, A. Gujral, B. Kahr, *Angew. Chem., Int. Ed.* **2014**, *53*, 672; b) L. Catalano, J. Berthaud, G. Dushaq, D. P. Karothu, R. Rezgui, M. Rasras, S. Ferlay, M. W. Hosseini, P. Naumov, *Adv. Funct. Mater.* **2020**, *30*, 2003443.

[6] a) N. Chandrasekhar, M. A. Mohiddon, R. Chandrasekar, *Adv. Opt. Mater.* **2013**, *1*, 305; b) N. Chandrasekhar, R. Chandrasekar, *Chem. Commun.* **2010**, *46*, 2915; c) S. Basak, R. Chandrasekar, *Adv. Funct. Mater.* **2011**, *21*, 667.

[7] a) Y. S. Zhao, *Organic Nanophotonics: Fundamentals and Applications*, Springer, Berlin Heidelberg **2014**; b) R. Chandrasekar, *Phys. Chem. Chem. Phys.* **2014**, *16*, 7173; c) N. Mitetelo, D. Venkatakrishnarao, J. Ravi, M. Popov, E. Mamonov, T. V. Murzina, R. Chandrasekar, *Adv. Opt. Mater.* **2019**, *7*, 1801775; d) P. Hui, R. Chandrasekar, *Adv. Mater.* **2013**, *25*, 2963; e) N. Chandrasekhar, S. Basak, M. A. Mohiddon, R. Chandrasekar, *ACS Appl. Mater. Interfaces* **2014**, *6*, 1488; f) V. V. Pradeep, N. Mitetelo, M. Annadhasan, E. Mamonov, T. V. Murzina, R. Chandrasekar, *Adv. Opt. Mater.* **2020**, *8*, 1901317; g) Y. Zhang, Q. Liao, X. G. Wang, J. N. A. Yao, H. B. Fu, *Angew. Chem., Int. Ed.* **2017**, *56*, 3616; h) M. P. Zhuo, J. J. Wu, X. D. Wang, Y. C. Tao, Y. Yuan, L. S. Liao, *Nat. Commun.* **2019**, *10*, 9; i) X. Zhang, J.-J. Wu, H. Gao, Y. Zhao, W. Qi, J. Feng, X.-D. Wang, Y. Wu, L. Jiang, *Adv. Opt. Mater.* **2020**, *8*, 1901643; j) M.-P. Zhuo, G.-P. He, Y. Yuan, Y.-C. Tao, G.-Q. Wei, X.-D. Wang, S.-T. Lee, L.-S. Liao, *CCS Chem.* **2020**, *2*, 413.

[8] a) Y. C. Tao, X. D. Wang, L. S. Liao, *J. Mater. Chem. C* **2019**, *7*, 3443; b) D. Venkatakrishnarao, R. Chandrasekar, *Adv. Opt. Mater.* **2015**, *4*, 112; c) D. Venkatakrishnarao, E. V. Mamonov, T. V. Murzina, R. Chandrasekar, *Adv. Opt. Mater.* **2018**, *6*, 1800343; d) K. Tabata, D. Braam, S. Kushida, L. Tong, J. Kuwabara, T. Kanbara, A. Beckel, A. Lorke, Y. Yamamoto, *Sci. Rep.* **2014**, *4*, 5902; e) J. Ravi, D. Venkatakrishnarao, C. Sahoo, S. R. G. Naraharisetty, N. Mitetelo, A. A. Ezhov, E. Mamonov, T. Murzina, R. Chandrasekar, *ChemNanoMat* **2018**, *4*, 764; f) D. Venkatakrishnarao, C. Sahoo, E. A. Mamonov, I. A. Kolmychek, A. I. Maydykovskiy, N. V. Mitetelo, V. B. Novikov, S. R. G. Naraharisetty, T. V. Murzina, R. Chandrasekar, *J. Mater. Chem. C* **2017**, *5*, 12349.

[9] a) W. Zhang, J. Yao, Y. S. Zhao, *Acc. Chem. Res.* **2016**, *49*, 1691; b) X. Wang, Q. Liao, H. Li, S. Bai, Y. Wau, X. Lu, H. Hu, Q. Shi, H. Fu, *J. Am. Chem. Soc.* **2015**, *137*, 9289; c) X. Wang, Q. Liao, Q. Kong, Y. Zhang, Z. Xu, X. Lu, H. Fu, *Angew. Chem.* **2014**, *126*, 5973; d) D. Venkatakrishnarao, Y. S. L. V. Narayana, M. A. Mohaiddon, E. A. Mamonov, I. A. Kolmychek, A. I. Maydykovskiy, V. B. Novikov, T. V. Murzina, R. Chandrasekar, *Adv. Mater.* **2017**, *29*, 1605260.

[10] a) K. Takazawa, J. Inoue, K. Mitsuishi, T. Kuroda, *Adv. Funct. Mater.* **2013**, *23*, 839; b) K. Takazawa, J.-I. Inoue, K. Mitsuishi, T. Takamasu, *Adv. Mater.* **2011**, *23*, 3659; c) C. Zhang, C.-L. Zou, Y. Zhao, C.-H. Dong, C. Wei, H. Wang, Y. Liu, G.-C. Guo, J. Yao, Y. S. Zhao, *Sci. Adv.* **2015**, *1*, e1500257.

[11] G. Zhao, H. Dong, Q. Liao, J. Jiang, Y. Luo, H. Fu, W. Hu, *Nat. Commun.* **2018**, *9*, 4790.

[12] D. Venkatakrishnarao, M. A. Mohiddon, N. Chandrasekhar, R. Chandrasekar, *Adv. Opt. Mater.* **2015**, *3*, 1035.

[13] H. Zhang, H. Liu, Z. Lu, B. Tang, C. Qu, Z. Zhang, *Angew. Chem., Int. Ed.* **2020**, *59*, 12944.

[14] a) S. Basak, R. Chandrasekar, *J. Mater. Chem. C* **2014**, *2*, 1404. b) U. Venkataramudu, D. Venkatakrishnarao, N. Chandrasekhar, M. A. Mohiddon, R. Chandrasekar, *Phys. Chem. Chem. Phys.* **2016**, *18*, 15528. . c) M. Annadhasan, D. P. Karothu, R. Chinnasamy, L. Catalano, E. Ahmed, S. Ghosh, P. Naumov, R. Chandrasekar, *Angew. Chem., Int. Ed.* **2020**, *59*, 13821; d) M. Annadhasan, A. R. Agrawal, S. Bhunia, V. V. Pradeep, S. S. Zade, C. M. Reddy, R. Chandrasekar, *Angew. Chem., Int. Ed.* **2020**, *59*, 13852; e) M. Annadhasan, S. Basak, N. Chandrasekhar, R. Chandrasekar, *Adv. Opt. Mater.* **2020**, *8*, 2000959; f) M. Annadhasan, A. Vinod Kumar, D. Venkatakrishnarao, E. A. Mamonov, R. Chandrasekar, *Nanoscale Adv.* **2020**, *2*, 5584.

[15] a) D. Cáceres, C. Cebrián, A. M. Rodríguez, J. R. Carrillo, A. Díaz-Ortiz, P. Prieto, F. Aparicio, F. García, L. Sánchez, *Chem. Commun.* **2013**, *49*, 621; b) M. J. Pastor, I. Torres, C. Cebrián, J. R. Carrillo, A. Díaz-Ortiz, E. Matesanz, J. Buendía, F. García, J. Barberá, P. Prieto, L. Sánchez, *Chem. – Eur. J.* **2015**, *21*, 1795. c) R. Martín, P. Prieto, J. R. Carrillo, I. Torres, C. A. Strassert, K. Soloviova, A. M. Rodríguez, L. Sánchez, A. Díaz-Ortiz, *Dyes Pigm.* **2018**, *151*, 327.

[16] N. H. Nordin, Z. Ahmad, *J. Phys. Sci.* **2015**, *26*, 11.